Journal of Sound and Vibration (2001) **244**(3), 505–534
doi:10.1006/jsvi.2000.3487, available online at http://www.idealibrary.com on IDEAL®

RADIATION IMPEDANCE OF TUBES WITH DIFFERENT FLANGES: NUMERICAL AND EXPERIMENTAL INVESTIGATIONS

J.-P. DALMONT

Institut d'Acoustique et de Mécanique, Laboratoire d'Acoustique de l'Université du Maine (UMR CNRS 6613), *Avenue Olivier Messiaen*, 72085 *Le Mans Cedex* 9, *France.*
E-mail: *jean-pierre.dalmont@univ-lemans.fr*

C. J. NEDERVEEN

Acacialaan 20, 2641 *AC Pijnacker*, *The Netherlands*

AND

N. JOLY

Institut d'Acoustique et de Mécanique, Groupe Transfert Vibratoire, *Avenue Olivier Messiaen*, 72085 *Le Mans Cedex* 9, *France*

(*Received* 9 *March* 2000, *and in final form* 20 *November* 2000)

End corrections for open-ended cylindrical tubes are determined theoretically and experimentally. For the zero and low frequencies, the wave equation is solved numerically by using a finite difference method. For higher frequencies the complex radiation impedance is measured and for circular flanges, calculated with the boundary element method. For low frequencies the BEM links up with the FDM and for higher frequencies fits with experimental results. Various flanges found in particular in musical instruments are considered: circular flanges of various sizes, spherical and cylindrical flanges, square flanges, the normalised flange (used for loudspeaker testing), short flaring horns and a disk at a certain distance above the open end. Analytical fit formulas are proposed for each case.

1. INTRODUCTION

The radiation impedance of an open-ended tube has a small but finite value. Its imaginary part acts as an end correction to the geometrical tube length from which the resonance frequency of the tube is calculated. Accurate knowledge of the value of this end correction is important in the case of wind musical instruments, since differences of 0·1% in frequency are musically significant. The magnitude of this end correction depends on details of the geometry of the open end. Exact theoretical values are available only for two extreme situations namely for a cylinder with a circular flange of infinite and of zero dimensions [1–3]. The length correction for low frequencies in these two cases is 0·8216a and 0·6133a, respectively, where a is the inner radius of the cylinder. As these limit cases do not correspond to realistic situations on wind instruments, the knowledge of the values for other sizes and shapes is of particular interest. For a circular flange of finite dimensions the value will most likely be somewhere in between those for the two extreme cases, but this statement is not sufficiently accurate. For other geometries the value is difficult to estimate: it might be

0022-460X/01/280505 + 30 $35.00/0

outside this range, for example for a disk at a small distance from the open end (key above a hole) it is expected to be larger than the infinite-flange value.

Sound levels in wind instruments can be high and a mean flow is superimposed on the acoustic one. This can cause non-linear effects, such as shock waves [4], vortex formation [5] and large losses due to a pressure drop at a diameter change [6]. Although these effects can be important in practical situations, they will not be considered in the present study which is restricted to small-amplitude linear acoustics.

The need for more accurate values has prompted investigations, reported in the literature. Benade and Murday [7] and Peters *et al.* [5] experimentally investigated cylindrical flanges of various diameters. Ando [8] and later, Bernard and Denardo [9] analytically investigated circular flanges in the range of the ratio of tube and flange radius, a/b, from 0·7 to 1. For other geometries commonly found on wind musical instruments such as a disk at a certain distance of an open end, and holes drilled in a cylindrical wall (recorder), results have been reported [7, 10–12] and summarized by Nederveen [12].

The aim of this paper is to determine the end corrections for a number of geometries found in woodwinds (see Figure 1) with a precision sufficient for calculation of the resonance frequency within the above-mentioned limit. Approaches considered were analytical, numerical (the finite difference method—FDM and the boundary element method—BEM) and experimental. The analytical method seems promising in the case of the circular flange on a cylindrical tube. This would mean extending the approach of Ando [8, 9], i.e., using the Wiener–Hopf technique. However, when taking more terms of the expansion into account the number of functions to be determined increases rapidly. The number of terms necessary is probably larger, considering the fact that the last term in the calculations of Ando [8, 9] is still 20% of the total length correction. This route was abandoned. Instead, numerical approaches and experiments were chosen, for the circular flanges as well as for the other geometries.

For the experiments an accurately calibrated impedance sensor was employed. Two different methods were used. One measures the complex impedance of a short tube and gives the radiation impedance as a function of frequency (section 3.3.1). The other measures the resonance frequencies of the tube before and after variation of the end geometry and gives the radiation impedance at one frequency (section 3.3.2).

Figure 1 shows the various geometries investigated. Thin and thick circular flanges (Figure 1(a) and 1(b), respectively), were studied with BEM, FDM and experiments: real and imaginary parts versus frequency were determined (section 4). The case of the normalized flange (Figure 1(d)), used for loudspeaker characterization (section 5.2), as well as the spherical and cylindrical flanges (Figure 1(e) and 1(f), respectively, section 6) and short flaring horns (Figure 1(g) section 7), were investigated with both FDM and experiments based on impedance measurements. The cases of solid and perforated disks hanging above holes (Figures 1(h) and 1(i)) were investigated with both FDM and experiments based on resonance frequency measurements (section 8). The case of a square flange on a square tube (Figure 1(c)) has been investigated only with FDM (section 5.1). The nomenclature is given in Appendix A.

2. GENERALITIES

2.1. DEFINITIONS

2.1.1. *Reflection coefficient*

For a plane wave propagating in the positive direction in a cylindrical straight tube the reflection coefficient R_x at a given abscissa is the ratio of the reflected wave p_- and the

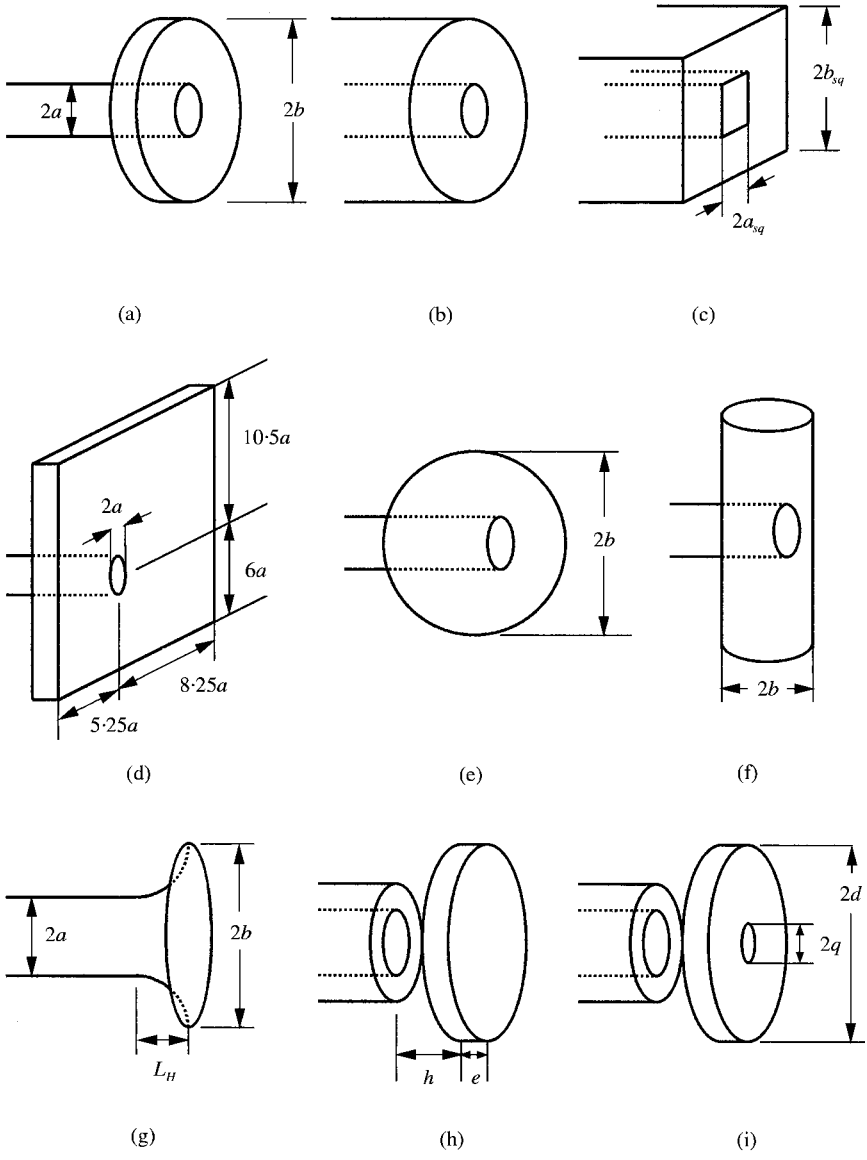

Figure 1. Shapes investigated: (a) thin circular flange; (b) thick circular flange or thick tube; (c) thick square tube; (d) the normalized flange; (e) spherical flange; (f) cylindrical flange; (g) short catenoidal horn; (h) non-perforated disk; (i) perforated disk.

incident wave p_+ at this abscissa:

$$R_x = p_-/p_+ \tag{1}$$

At the end of an open tube the wave front is no longer plane and this definition cannot be applied. Instead, the reflection coefficient R_0 at the end of the tube ($x = 0$) is defined from the reflection coefficient R_L at a distance L, inside the tube ($x = -L$), from the open end so that the front wave is plane

$$R_0 = R_L \mathrm{e}^{2\mathrm{j}kL}, \tag{2}$$

where k is the complex wave number. Note that, for an open end, this reflection coefficient is negative and that the $e^{j\omega t}$ convention is used for the time dependence.

In practice, to ensure a plane wave front under the first cut-off frequency, the distance L needs to be only larger than 2 or 3 times the diameter of the tube. The first cut-off frequency being given by $ka = 1{\cdot}84$, with k the wave number and a the radius of the tube, this will be valid for $ka < 1$ or even $< 1{\cdot}5$.

For sufficiently large tubes with rigid and smooth walls the wave number k is given by

$$k = (\omega/c) + (1 - j)\,\alpha, \tag{3}$$

where c is the speed of sound, $\omega = 2\pi f$ with f the frequency, j is the square root of minus one and α is given by

$$\alpha = \frac{1}{a}\sqrt{\frac{\omega}{2c}}\,(\sqrt{\ell_v} + (\gamma - 1)\sqrt{\ell_h}), \tag{4}$$

where ℓ_v and ℓ_h are the characteristic lengths for viscous and thermal effects respectively. γ is the ratio of the specific heats of air at constant pressure and constant volume (see for example, references [13, 14]).

For air Caussé *et al.* [15] proposed the following formula for α:

$$\alpha = 2{\cdot}87 \times 10^{-5}\,(1 + 0{\cdot}0016t)\,\sqrt{f}/a \tag{5}$$

with t the temperature in $^\circ$ Celsius, a the radius in m and f the frequency in Hz. This formula has been verified experimentally to be accurate within $\pm$ 3% [16].

2.1.2. *Radiation impedance*

The impedance Z is related to the reflection coefficient R according to the relation

$$Z = Z_c\,(1 + R)/(1 - R), \tag{6}$$

where Z_c is the characteristic impedance of the tube. For a large tube the influence of damping on Z_c can be neglected. Z_c is approximately given by

$$Z_c \approx \rho c/S, \tag{7}$$

where ρ is the density of air, c the speed of sound and S the cross-section of the tube. In practice, the impedance at the tube end, the radiation impedance Z_r cannot be calculated or measured at the end of the tube. It must be evaluated indirectly from the impedance Z_L at an abscissa $x = -L$, i.e., at a distance L from the open end. This is, upon using equations (2) and (6), given by

$$Z_L = jZ_c \tan\,[kL + \arctan\,(Z_r/jZ_c)]. \tag{8a}$$

So the radiation impedance can be defined as that impedance yielding an input impedance for a tube of length L as given by equation (8a). This means that it can be determined from the impedance at a distance $-L$ from the end by using the following formula derived from equation (8a):

$$Z_r = jZ_c \tan\,[\arctan\,(Z_L/jZ_c) - kL]. \tag{8b}$$

2.1.3. *Length correction*

Upon writing $\tilde{\delta}^* = k^{-1}\,\arctan[Z_r/(j\,Z_c)]$ equation (8a) becomes

$$Z_L = j\,Z_c \tan[k(L + \tilde{\delta}^*)]. \tag{9}$$

$L + \tilde{\delta}^*$ is the "effective" acoustical length of the tube; i.e. the length of a tube terminated with a zero impedance of the same input impedance. Notice that it could also be referred to as a tube terminated with an infinite impedance (see reference [17]) which defines another length correction. Equation (9) defines the end correction as a complex (superscript $*$) and frequency-dependent quantity (upper script $\sim$). Most of the considerations in the present paper consider only the real part of the length correction:

$$\tilde{\delta} = \mathrm{Re}\,(\tilde{\delta}^*). \tag{10}$$

The resonance frequencies of a one-sides open tube, if $\mathrm{Im}(k)\ \mathrm{Im}(\tilde{\delta}^*)$ is not too large, are given by

$$f_n = (2n + 1)\, c(\omega)/4(L + \tilde{\delta}) \tag{11}$$

with $c(\omega) = \omega/\mathrm{Re}(k)$ and $n = 1, 2, 3, \ldots$

Although $\tilde{\delta}$ is frequency dependent, it is a useful quantity because it is approximately constant for low frequencies ($ka < 0{\cdot}2$). The length correction considered in the present paper is valid for a straight tube: for a horn, for example, it is only an approximation.

The reflection coefficient can also be written by using the following formula derived from equations (6) and (9):

$$R_0 = -\,\mathrm{e}^{-2\mathrm{j}k\tilde{\delta}^*} = -\,|R_0|\,\mathrm{e}^{-2\mathrm{j}k\tilde{\delta}}. \tag{12}$$

2.2. THEORETICAL RESULTS FOR AN INFINITE FLANGE AND AN UNFLANGED PIPE

2.2.1 *Unflanged pipe*

The end correction for an unflanged pipe has been calculated by Levine and Schwinger [2]. As they do not give simple formula for low frequencies it is convenient to use approximate formulas. Caussé *et al.* [15] proposed the following expression for the impedance:

$$Z_0/Z_c = \mathrm{j}k\delta_0 - \mathrm{j}(ka)^3\,[0{\cdot}036 - 0{\cdot}034\ln(ka) + 0{\cdot}0187(ka)^2] + (ka)^2/4 + (ka)^4\,[0{\cdot}0127 + 0{\cdot}082\ln(ka) - 0{\cdot}023(ka)^2] \quad \text{for } ka < 1{\cdot}5. \tag{13}$$

Here $\delta_0 = 0{\cdot}6133a$, with a the inner radius of the tube. The accuracy is given to be better than 1%.

For the same case Norris and Sheng [18] proposed a simple approximate formula for the equivalent length:

$$\tilde{\delta}_0 = \delta_0\,\frac{1 + 0{\cdot}044(ka)^2}{1 + 0{\cdot}19(ka)^2} \quad \text{for } ka < 3{\cdot}5. \tag{14a}$$

This formula is not as accurate as the one given in reference [15]. The accuracy is only 3%. To obtain a better accuracy (1%) for $ka < 1{\cdot}5$ the present authors propose to add a corrective term; i.e., to use the formula

$$\tilde{\delta}_0 = \delta_0\left[\frac{1 + 0{\cdot}044(ka)^2}{1 + 0{\cdot}19(ka)^2} - 0{\cdot}02\sin^2(2ka)\right] \quad \text{for } ka < 1{\cdot}5. \tag{14b}$$

For the modulus of the reflection coefficient one has [18]

$$|R_0| = \frac{1 + 0{\cdot}2ka - 0{\cdot}084(ka)^2}{1 + 0{\cdot}2ka + (\tfrac{1}{2} - 0{\cdot}084)(ka)^2} \quad \text{for } ka < 3{\cdot}5. \tag{14c}$$

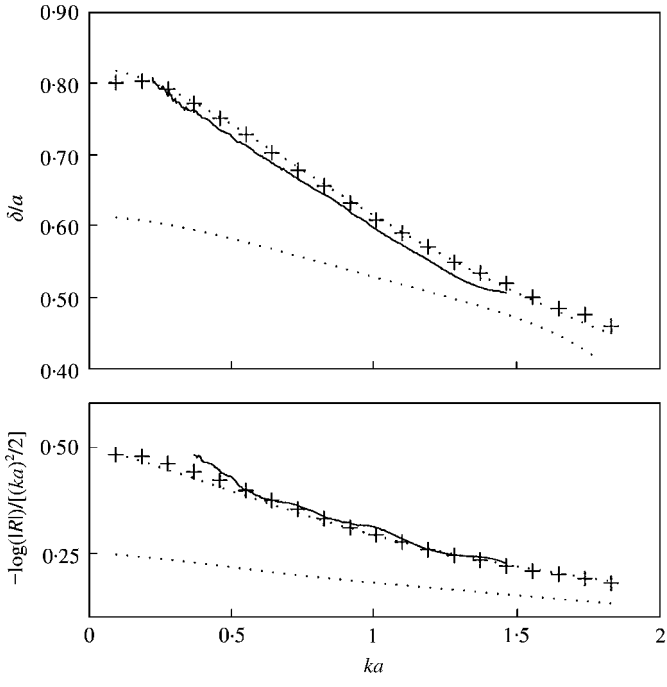

Figure 2. Radiation impedance versus frequency for the infinitely and unflanged case (equations (15) and (13), respectively), and the normalized flange. upper; length correction δ over inner radius a; lower; absolute value of the logarithm of the modulus of the reflection coefficient over $(ka)^2/2$. ·····, Theory for infinite flange [upper, equation (15)] and unflanged case [lower, equation (13)]; $+++$, calculation with BEM for the infinite flange; ——, experimental results for the normalized flange (see Figure 1(d) and section 5.2).

These equations are plotted in Figure 2 with a dotted line. Note that $\ln(|R_0)|/[(ka)^2/2]$ tends to 0·25 when frequency tends to zero.

2.2.2. *Infinite flange*

The end correction for a tube with an infinite flange has been calculated by Nomura *et al.* [3]. Norris and Sheng [18] derived a simpler form and gave the following fit formulas for $ka < 3{\cdot}5$:

$$\tilde{\delta}_\infty = \delta_\infty \left[1 + \frac{(0{\cdot}77ka)^2}{1 + 0{\cdot}77ka}\right]^{-1} \tag{15a}$$

with $\delta_\infty = 0{\cdot}8216a$ with a the inner radius of the tube, and

$$|R_\infty| = \frac{1 + 0{\cdot}323ka - 0{\cdot}077(ka)^2}{1 + 0{\cdot}323ka + (1 - 0{\cdot}077)(ka)^2}. \tag{15b}$$

These equations are plotted in Figure 2 with a dotted line. Note that $\ln(|R_0)||[(ka)^2/2]$ tends to 0·5 when the frequency tends to zero.

3. INVESTIGATION METHODS

The theoretical investigations consisted of two numerical methods, the finite difference method (FDM) for $ka \leqslant 0{\cdot}15$ and the boundary element method (BEM) for $ka \geqslant 0{\cdot}18$. The

experiments consisted of impedance and resonance frequency measurements. The numerical methods are based on the linear acoustic equations without dissipation in a homogeneous acoustic fluid (speed of sound c, density ρ). The 3-D domain considered is denoted by Ω, and its boundaries are denoted by Γ.

For the harmonic regime at wave number $k = \omega/c$, the local equation (16) has to be satisfied in the domain Ω:

$$\nabla^2 p + k^2 p = 0 \quad \text{in the domain } \Omega. \tag{16}$$

The boundary conditions are an imposed normal velocity V_0 at the boundary Γ of the domain Ω:

$$\partial p/\partial n = \mathrm{j}\omega\rho V_0 \quad \text{on } \Gamma \tag{17}$$

and the Sommerfeld condition at infinity

$$\lim_{r\to\infty} r\,(\partial p/\partial r + \mathrm{j}kp) = 0. \tag{18}$$

3.1. FINITE DIFFERENCE METHOD (FDM)

The finite difference method can be used for obtaining numerical approximation for differential equations in a domain with specified boundary conditions. In the domain a collection of points is defined forming a grid or mesh. Computational "molecules" are formed consisting of neighbouring points, for which difference schemes are set-up. This results in a set of linear equation for the pressures in all points, which subsequently can be solved. The accuracy is determined by the number of points of the grid. The method has no systematic error. Since the study concerns cylindrical tubes, it is advantageous to express the Helmholtz (wave) equation (16) for the pressure p in cylindrical co-ordinates:

$$\frac{1}{r}\frac{\partial}{\partial r}\left(r\frac{\partial p}{\partial r}\right) + \frac{1}{r^2}\frac{\partial^2 p}{\partial \varphi^2} + \frac{\delta^2 p}{\partial z^2} + k^2 p = 0. \tag{19}$$

Figure 3 shows a computational module of the 3-D discretization grid. The cylinder axis is parallel to the top-bottom direction, the centreline is in the 'western" direction.

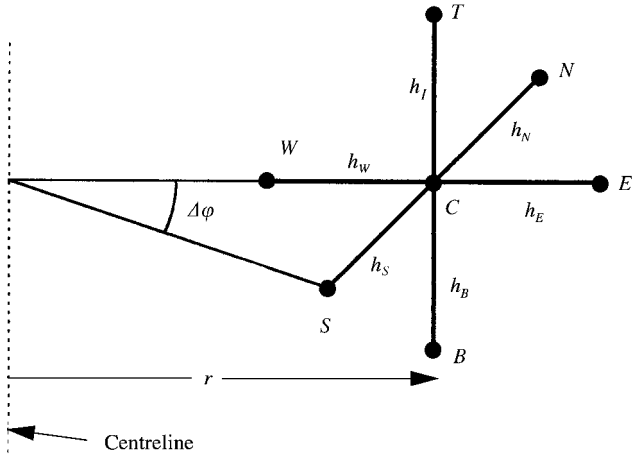

Figure 3. Discretization grid for a computational "molecule".

In the plane perpendicular to the centreline, the central point C is surrounded by points to the north (N), the south (S), the west (W) and the east (E), and in the plane through the centreline, to the top (T) and the bottom (B). The grid size is denoted by h with an index corresponding to the direction. The radius of curvature in the central point is r. The discretization equations for the four terms of equation (19) are [19, 20]

$$\frac{1}{r}\frac{\partial}{\partial r}\left(r\frac{\partial p}{\partial r}\right)=\frac{2}{r(h_W+h_E)}\left[r\left(1-\frac{h_W}{2r}\right)\frac{p_W-p_C}{h_W}+r\left(1+\frac{h_E}{2r}\right)\frac{p_E-p_C}{h_E}\right], \tag{20}$$

$$\frac{1}{r^2}\frac{\partial^2 p}{\partial \varphi^2}=\frac{2}{h_N+h_S}\left(\frac{p_N-p_C}{h_N}+\frac{p_S-p_C}{h_S}\right), \tag{21}$$

$$\frac{\partial^2 p}{\partial z^2}=\frac{2}{h_T+h_B}\left(\frac{p_T-p_C}{h_T}+\frac{p_B-p_C}{h_B}\right), \quad k^2 p=k^2 pc. \tag{22, 23}$$

The points of the grid are situated in planes through the axis. These planes are angles of $\Delta\varphi$ apart in the φ direction, so $h_N=h_S=r\Delta\varphi$.

The boundary conditions are mixed. Where the flow is parallel to the boundary, the derivative normal to the wall is zero: $\partial p/\partial n=0$ (equation (17)). This means that the term for the outside (virtual) point disappears, and that in the term for the inside point the grid dimension of the value of the outside-h is zero. In the case of a uniformly sized grid this means that the contribution of the inside point (perpendicular to the wall) is doubled. At the entrance points of the tube, the value of the pressure is specified. In principle, the outside region stretches to infinity, where the pressure gradually vanishes with increasing distance, becoming zero at infinity. In practice, this "infinity" can be limited to a distance where the results do not vary by more than a prescribed accuracy upon varying this distance. Even then this demands a large computer capacity. Various measures of reducing the number of equations are possible.

The first and obvious step in reducing the number of equations is the use of the cylindrical symmetry. This reduces the problem to a two-dimensional one with axial symmetry. Then the terms with φ disappear, or equation (21) can be left out. For the case where all grids are of the same size, the discretized Helmholtz equation becomes

$$(1+h/2r)(p_E-p_C)+(1-h/2r)(p_W-p_C)+(p_T-p_C)+(p_B-p_C)+k^2 p_C=0. \tag{24}$$

In the centreline, where $r=0$, in equation (20) some terms become infinitely large, making it undetermined. This can be circumvented as follows [21]. In the centreline ($r=0$) the derivative in the r direction of the pressure is assumed to be zero, or $\partial p/\partial r\,(0)=0$. Adding this term of equation (20) gives

$$\frac{1}{r}\frac{\partial}{\partial r}\left(r\frac{\partial p}{\partial r}\right)=\frac{1}{r}\left(\frac{\partial p}{\partial r}(r)-\frac{\partial p}{\partial r}(0)\right)+\frac{\partial^2 p}{\partial r^2}(r). \tag{25}$$

In the limit of $r\to 0$, the first term on the right-hand side is equivalent to the definition of the second derivative of p to r. So, for $r=0$, the right-hand side of the expression becomes $2(\delta^2 p/\partial r^2)(0)$. Because of cylindrical symmetry, only the part east of the centreline needs to be considered, or $p_W=p_E$. The discretization equation for points around the centreline now becomes

$$4(p_E-p_C)+(p_T-p_C)+(p_B-p_C)+k^2 p_C=0. \tag{26}$$

The problem now is formulated as a linear system of equations for the pressures in the mesh points. The resulting matrix equation can be solved (by using a computer) by standard techniques, either directly or by relaxation.

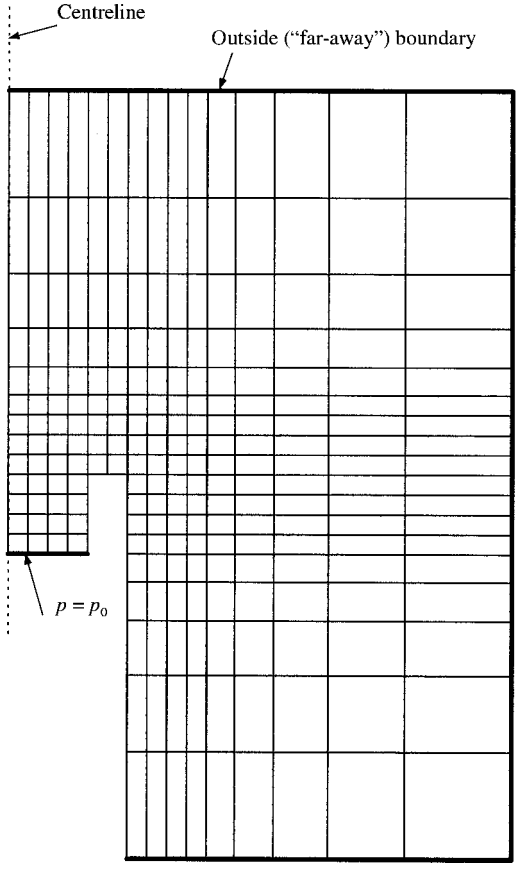

Figure 4. Example of grid for hole with flange, stretching into space.

The effective length of the tube is obtained from the input impedance of the combination looking into the tube, which is calculated from the mean value of the gradient at the tube entrance plane. From this the end correction is calculated by comparision with that of a straight cylinder with a zero terminating impedance. To illustrate the procedure consider the case of zero frequency, where $k = 0$. The pressure gradient $\partial p/\partial x$ at the entrance of the tube is related to the pressure p_0 (or velocity potential) at the tube entrance, and the length of the tube, L, including its end correction δ at the radiating open end by

$$\partial p/\partial x = -p_0/(L + \delta). \tag{27}$$

In the present calculation, p_0 was set to 1.

A further reduction of the number of equations is obtained by limiting the length of the cylindrical tube part. It was verified that taking this length equal to the radius caused an error of less than 0·01% in the end correction.

Figure 4 shows an example of a grid in a particular situation. The boundaries at which the pressure values are prescribed are indicated by thick lines. At boundaries with thin lines the normal velocity vanishes. In this example another saving measure is shown, namely stepwise increasing the grid spacing (here with a factor of 1·4) starting at a certain distance from the tube end.

The next equations-saving measure uses the fact that at a sufficiently large distance and sufficiently low frequency (in this paper $ka \leqslant 0{\cdot}15$), the field becomes practically identical to

that of a spherical source. For such a field (with assumed strength U) the pressure at a distance R from the source $p(R) = (\rho\,(\mathrm{d}U/4\pi R)\,\mathrm{d}t)$ [22, p. 155] or $p(R) = A/R$, where A is a constant determined by

$$\rho\,\mathrm{d}U/\mathrm{d}t = 4\pi A. \tag{28}$$

In the present configuration the source is formed by the open end of the cylindrical tube with radius a, the flow (volume velocity) U existing the tube is found from

$$\rho\,\mathrm{d}U/\mathrm{d}t = \pi a^2\,\partial p/\partial x. \tag{29}$$

Setting the pressure at an outside boundary at a distance R equal to A/R and combining equations (27)–(29) gives a relationship between A and δ:

$$A = p_0\,a^2/4(L + \delta). \tag{30}$$

To solve this for the two unknowns A and δ a second conditions is necessary. This can be obtained by using an estimate for A and calculation the gradient for two values of R, plotting $\partial p/\partial x$ versus $1/R$ and extrapolating to zero. Assume the estimate for A to be $A + \alpha$. This means that the value at the boundary is an amount α/R too high, due to which the pressure drop between the tube entrance and the boundary diminishes by the same amount.

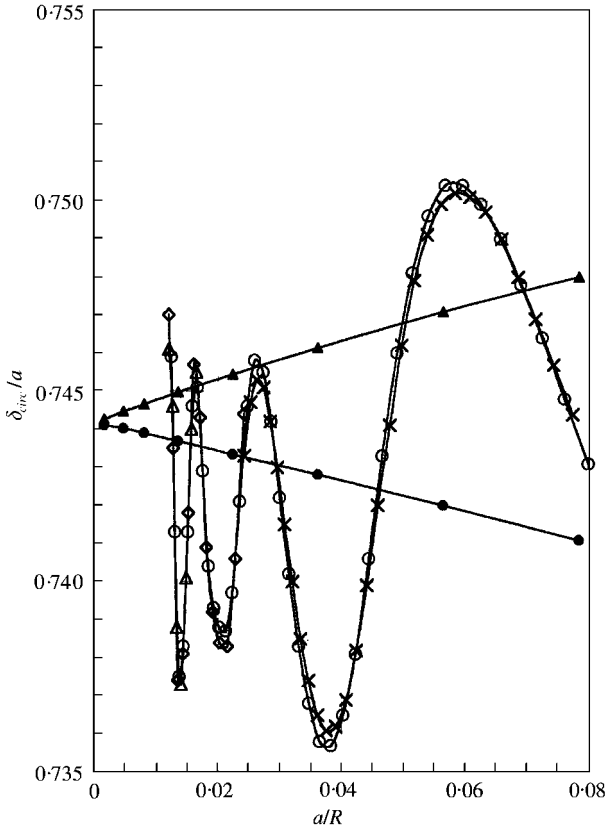

Figure 5. Plots of the real part of the end correction coefficient δ/a for a flat circular flange as a function of a/R, where a = cylinder radius, R = distance to the "far" boundary and k = wave number. ▲, $ka = 0$, $A = 0{\cdot}27a$; ●, $ka = 0$, $A = 0{\cdot}18a$; ×, $ka = 0{\cdot}15$, grid stretch = 4%; ○, $ka = 0{\cdot}15$, grid stretch = 5%; △, $ka = 0{\cdot}15$, grid stretch = 5·5%; ◇, $ka = 0{\cdot}15$, grid stretch = 6%.

So the pressure value at the tube entrance becomes $p_0 - \alpha/R$ instead of p_0, due to which equation (27) changes into

$$\frac{\partial p}{\partial x} = \frac{-p_0}{L+\delta} + \frac{\alpha}{L+\delta} \times \frac{1}{R}. \tag{31}$$

Extrapolating the value of $\partial p/\partial x$ to zero in a plot of $\partial p/\partial x$ against $1/R$ gives $p_0/(L+\delta)$, from which δ is obtained since p_0 is given. For greater accuracy, and to verify the absence of nearfield effects, more than two values of R were taken. Alternatively, δ can be plotted directly versus $1/R$. Figure 5 shows two examples of plots of δ/a versus a/R, for $a/b = 0{\cdot}5$, where $L = a = 15$ mesh points, and $A = 0{\cdot}18a$ and $0{\cdot}27a$ respectively. The network stretch was varied between 2 and 10% over 70 points. Lines through the points appear to be nearly straight and both cut the vertical axis at approximately $\delta/a = 0{\cdot}7442$. To estimate the possible error, several calculations with varying choices of the network parameters were made. It was found that the results were the same within $\pm 0{\cdot}001$, provided the number of points over the radius was more than 10, and $L \geqslant a$. Similar results were observed for other flange sizes. It seems justified to state that the results obtained with the finite difference method deviate less than 0·005 from the real values.

When the wave number k is complex, pressure values become complex and prescribing the conditions at the outside boundaries as real values is not correct. Instead, Sommerfeld's condition must be used (equation (18)). In the grid used, where most of the mesh lines are not in the R direction, this condition takes on the form

$$\partial p/\partial n = \mathrm{j}kp. \tag{32}$$

Since the tube is no longer a pure acoustic mass, equation (27) has to be modified as follows:

$$\partial p/\partial x = -k\,p_0/\tan(kL + k\delta). \tag{33}$$

The solutions obtained are complex, so the obtained end correction is also complex. This gives the end correction as well as the term in the radiation impedance related to the losses.

An example of results obtained is shown in Figure 5 for the same parameters as a in the example for zero frequency, except now the Helmholtz number $ka = 0{\cdot}15$. By applying various amounts of stretch and a varying number of points in the stretched part of the network, various distances to the boundary were created. The results plotted in Figure 5 appear to oscillate, the amplitude initially decreasing for increasing R. The wavelength of the oscillation appears to be related to an integer number of wavelengths to the boundary. One wavelength means $kR = 2\pi$, or $a/R = 0{\cdot}15/2\pi = 0{\cdot}24$. The pattern repeats when this number is halved or doubled. Apparently, the remaining reflections from the boundary are causing the fluctuations. For low values of ka, the oscillations were found to damp out sufficiently with increasing R to allow the establishment of a trustworthy value for the end correction. For the ka in the present example, however, the oscillation amplitude grows again with increasing distance. Most likely this is caused by the mesh dimensions becoming comparable to the wavelength, rendering the discrete approximation for the wave equation inaccurate. In the present case, the Helmholtz number for one non-stretched mesh unit is $0{\cdot}15/15 = 0{\cdot}01$; for a stretch of 6% over 70 steps it is $(1{\cdot}06)^{70} = 60$, so the Helmholtz number of the final mesh is $60 \times 0{\cdot}01 = 0{\cdot}6$, signifying that the sine or tangent of this number is not the same as the argument any more. A larger computer capacity would be needed to obtain more accurate numbers. In the present study, the value obtained for the end correction coefficient will be between 0·735 and 0·75, the most likely value being 0·742, definitely lower than the one for zero frequency.

The values for the extremes $a/b = 0$ and 1 are known from theory; calculating these with the FDM is a valuable check on the method. For $a/b = 1$, a series of calculations was done for a wall thickness of 1 element (the minimum value) and an increasing number of elements for the radius. Each radius value corresponded to a value of a/b. The end correction obtained was plotted versus its corresponding a/b value and extrapolated to $a/b = 1$. The value obtained appeared to equal the analytical value. For $a/b = 0$, the program was modified. The tube radiated into a half-infinite space or rather into the inside of a half-sphere. The flat hard wall of this half-sphere had a circular hole of radius a in its centre. The radius of the sphere was equal to the flange radius b. On its spherical wall the function value was set to A/R. Upon varying b, for a given value of a, end correction coefficients were obtained for various values of a/b. The value extrapolated to zero was, within uncertainty, equal to the theoretical value.

As remarked above, the program also produces values for the lossy part of the impedance. However, the amplitudes of the fluctuations were much larger. It was difficult to find accurate answers other than the fact that the term is between $(ka)^2/2$ and $(ka)^2/4$, the extreme values for infinite and zero flange respectively.

3.2. BOUNDARY ELEMENT METHOD (BEM)

The boundary element method (BEM) is based on writing the local equation (16) and the boundary conditions (17) and (18) from surface integrals on Γ. By discretization of the boundary in elements, these integrals can be numerically computed. The solution of this linear set of equations gives the pressure p on the surface Γ for the considered frequency.

The surface integral is obtained by using the Green function G

$$G(\mathbf{r}, \mathbf{r}_0) = \mathrm{e}^{-\mathrm{j}k|\mathbf{r}-\mathbf{r}_0|}/4\pi|\mathbf{r}-\mathbf{r}_0|, \tag{34}$$

which is the basic solution of the wave equation

$$\Delta G(\mathbf{r}, \mathbf{r}_0) + k^2 G(\mathbf{r}, \mathbf{r}_0) = -\delta(\mathbf{r}-\mathbf{r}_0), \tag{35}$$

where $\delta(\mathbf{r}-\mathbf{r}_0)$ is the Dirac function centred on $\mathbf{r}_0$, which satisfies the Sommerfeld condition

$$\lim_{r\to\infty} r\left(\frac{\partial G}{\partial r} + \mathrm{j}kG\right) = 0. \tag{36}$$

The Green theorem gives the integral relation

$$\int_\Gamma \left(p\frac{\partial G}{\partial n} - G\frac{\partial p}{\partial n}\right) \mathrm{d}\Gamma = \int_\Omega (p\nabla^2 G - G\nabla^2 p)\, \mathrm{d}\Omega.$$

From the wave equation and the Dirac properties, $\mathbf{r}_0$ pointing on any regular point of Γ, this surface integral can be written as

$$\int_\Gamma \left(G(\mathbf{r}, \mathbf{r}_0)\frac{\partial p(\mathbf{r})}{\partial n} - p(\mathbf{r})\frac{\partial G(\mathbf{r}, \mathbf{r}_0)}{\partial n_{\mathbf{r}}}\right) \mathrm{d}\Gamma(\mathbf{r}) = p(\mathbf{r}_0)/2 \quad \text{for every } \mathbf{r} \text{ in the } \Gamma \text{ domain,} \tag{37}$$

or, upon including the boundary condition (17),

$$\int_\Gamma \left(G(\mathbf{r}, \mathbf{r}_0)\,\mathrm{j}\rho\omega V_0 - p(\mathbf{r})\frac{\partial G(\mathbf{r}, \mathbf{r}_0)}{\partial n_{\mathbf{r}}}\right) \mathrm{d}\Gamma(\mathbf{r}) = p(\mathbf{r}_0)/2 \quad \text{for every } \mathbf{r} \text{ in the } \Gamma \text{ domain,} \tag{38}$$

where ρ, ω and the normal velocity U_0 on the boundary Γ are data introduced in the model, and $G(\mathbf{r}-\mathbf{r}_0)$ is the frequency-dependent Green function (34). Because of the singularity of

the Green function G and its normal derivatives when $\mathbf{r} \to \mathbf{r}_0$, the surface integrals (37) and (38) are defined in Cauchy's principal value sense.

In the BEM method, a mesh constituted of triangular and quadrangular elements discretizes the surface Γ. On the each element, the pressure field p on the boundary is interpolated by quadratic polynomials from the pressure values p_i of specific points, called "nodes". In the meshes used in this study, the nodes are the element's edge mid-points and end-points (six nodes belong to a triangular element, eight nodes to a quadrangular element).

A surface integral like the left-hand side member of equation (38) can then be computed by using Gauss integration, with a polynomial approximation for the Green function (34) and its normal derivative. Because of the behaviour of this function, the number of Gauss points used to complete the integration is increased when the distance $(\mathbf{r} - \mathbf{r}_0)$ decreases, and special techniques must be used when $\mathbf{r}_0$ and $\mathbf{r}$ are pointing to the same element.

In fact, two approximations are introduced in the exact integral form (38) by the boundary element method: the pressure field is represented by polynomial interpolation from discrete node values and this approximation is defined by the mesh; i.e. the element size and the total number of nodes; the computation of the surface integral, when using the Gauss integration technique, introduces an approximation of the Green function (34) [23].

Another problem is introduced by the integral form (38), presenting a non-unique solution for some discrete frequencies. At such "irregular frequencies", solutions of equation (38) may not be physical, introducing stationary waves between surface elements of Γ where there is no acoustic fluid between these surfaces. These irregular frequencies depend on the geometry of the model and the speed of sound c. The present study concerns simple geometrices for which irregular frequencies are predictable; therefore we were able to avoid computing acoustic responses at irregular frequencies corresponding to our model's geometry.

3.2.2. *Boundary element model definition*

The BEM models were computed by using the 3-D RAYON code, based on a variational formulation of the integral form (38) [24]. The components of the full square matrix are double integrals over the surface Γ, the second member is a simple integral over Γ. The node values of acoustic pressure on surface Γ are computed, which means solving a $n \times n$ linear set, n being the number of nodes of the mesh. Notice that when using boundary elements, the acoustic pressure is computed *on the surface only*, while pressure in the volume is not computed: the acoustic pressure on the surface of the piston is directly obtained.

When some symmetry planes exist, as is the case for circular flanges (see section 4), only one-quarter of the geometry is meshed, and the adapted Green function takes into account the symmetry [25]. Such an adaptive Green function can also take into account an infinite rigid baffle, without meshing it. This is used in section 2.2.2. for checking the accuracy of BEM calculations.

The modelled geometry is a circular tube of various thickness and length 100 mm. The source is modelled as a flat piston in the tube moving with a defined velocity. The back side of the piston is enclosed so that it radiates only on one side. In order to correctly interpolate the pressure field on the surfaces of the tube and of the flange, the boundary element models are defined by using curved elements. The meshes used are as regular as possible; both the inner and the outer side of the tube are meshed by quadrangles, the piston surface is meshed by triangular elements (see Figure 6).

The boundary conditions on rigid surface are $V_0 = 0$, except on the piston surface, where a finite normal velocity of unity is imposed. The model is of finite dimensions, the tube has

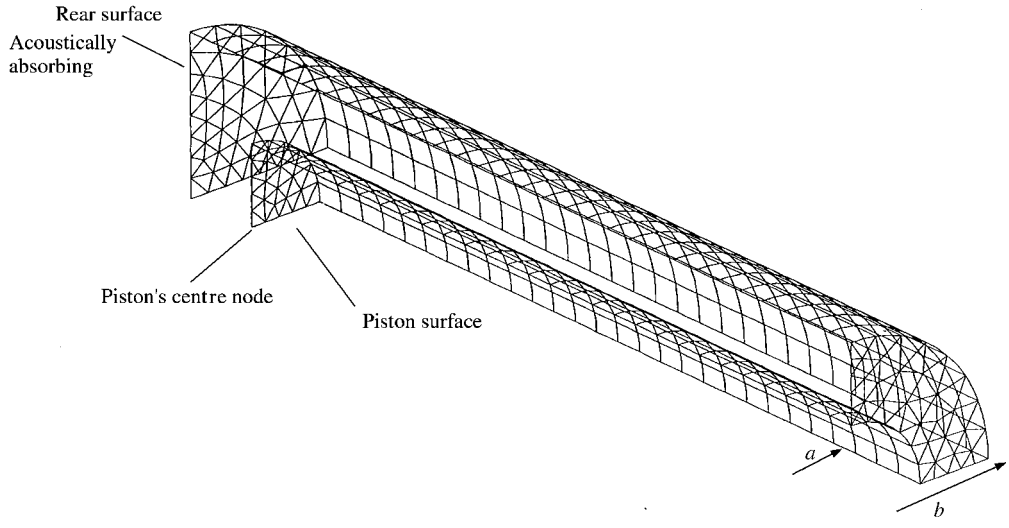

Figure 6. Mesh used for the boundary element model of a tube with a circular flange (case $a/b = 1/2$).

a finite length and is ended by a cylinder base. The cylinder base surface causes acoustic reflections on this rear surface. In order to minimize this effect, this rear surface is modelled as acoustically absorbing, with a specific impedance equal to unity.

The piston mesh has one node in its centre. After computation, for each frequency, the value of acoustic pressure at this point is obtained. Acoustic velocity being equal to unity, the radiation impedance is then deduced from this pressure, by using equation (8b).

The model, with two planes of symmetry and the acoustic pressures on surfaces used as unknowns was tested for the case of an infinite flange. Figure 2 shows that the difference between the theoretical curve and BEM calculations is small (less than 1%) except for low frequencies such that $ka < 0{\cdot}2$. This is probably due to numerical errors due to the low value of the pressure. Since this discrepancy appears to be the same for most situations, a correction g was added to the length correction for all results. By trial and error, this was found to be

$$g = 0{\cdot}027a/(1 + 75(ka)^2). \tag{39}$$

Less accurate results were obtained for situations for which plane symmetry does not exist as, for example, the normalized flange or the cylindrical flanges. Deviations were much larger than for the infinite flange.

3.3. EXPERIMENTS

2.3.1. *Impedance measurements*

The principle of the method is to measure the input impedance of a short tube of length L and of diameter $2a$ (usually L is the less than 100 mm and $a = 10$ mm) and to deduce from this impedance Z_L the radiation impedance Z_r by using equation (8b).

Despite the simplicity of this principles such a measure is not so easy to realize in practice. The first difficulty is caused by the fact that the dynamic range of the input impedance is large: it can be 80 dB between a maximum and a minimum. Measurements need to be

equally accurate for minima and maxima. Another difficulty is that the radiation impedance is not a very large effect: for plane flanges the low-frequency value of the length correction is between 0·61 and 0·82 times the radius. To obtain useful information on the length correction its value needs to be obtained with an accuracy of at least 1 or 2% of the radius. For a tube of the radius 10 mm such as the one used for the present experiments it means that the accuracy on the length correction must be one or two-tenth of a millimeter. All the dimensions need then to be measured accurately and the temperature has to be controlled as well. Such an accuracy can only be obtained with a painstakingly calibrated impedance sensor.

The impedance sensor used is based on the one described by Dalmont and Bruneau [26]. It uses a half-inch electrostatic microphone cartridge as a volume velocity source and one electret microphone. The microphone cartridge and the electret microphones are fixed in a metal plane which constitutes the reference plane for the measurements. The microphone and the source are placed as close as possible to the reference plane but some extra volume remains between the microphone membranes and the plane. The use of a microphone cartridge is attractive because its frequency response is rather flat and its mechanical impedance is relatively high. The limitation of this kind of source is that the volume velocity is proportional to the frequency and tends to zero when this frequency tends to zero. This makes measurements at low frequencies difficult. The measurements were carried out in an anechoic chamber with a dual-phase lock-in amplifier including a sine source used for both excitation and demodulation.

A precise calibration is important to minimize the error at every frequency and at every level. Details of the calibration procedure are given in reference [16]. It is based on the measurement of a long (1 m) and a short (0·085 m) tube, both closed. The calibration tubes are fixed on the measurement set-up with the same guiding tube which is not removed between experiments. All the flanges are fixed on the short calibration tube so that the diameter and position on the sensor are the same as that during the calibration. When different flanges have to be measured only the flanges are removed. Every manipulation is done with gloves to minimize temperature changes.

The final accuracy of measurement is determined by uncertainties in geometry and temperature. The length of the tube with a flange is measured together and the accuracy on the total length is estimated to be $\pm$ 0·05 mm. The error in the calibration parameters is estimated to be equivalent to $\pm$ 0·1 mm. This error is much higher for low frequencies and therefore this method cannot be used for low frequencies (for details see reference [16]). Temperature is measured with an accuracy of $\pm$ 0·3°C which leads to an equivalent length error of $\pm$ 0·05 mm for a 10 cm tube length. Total uncertainty on the equivalent length can then be as large as $\pm$ 0·2 mm. Besides, some unexpected errors can occur and only confrontation with an other estimation method can confirm the accuracy of the method.

3.3.2. *Resonance frequency measurements*

The resonance frequencies of a closed–open tube are given by equation (11). Measuring the first resonance frequency f_1, the temperature, and the length of the tube L gives the length correction

$$\tilde{\delta}(f_1) = \frac{c}{4f_1} - L. \tag{40}$$

This method gives the length correction at the first resonance frequency: it may differ from the low-frequency limit. However, it is a convenient method when determining the difference between different end geometries. In the present paper, it is used for the case of

a tube with a disk at a varying distance from the open end. The length correction is compared to the length correction without disk, which was previously determined with another method.

The length difference is assumed to be equivalent to the one at zero frequency. The same short tube was used as for impedance measurements (length 0·085 m) which means that errors due to temperature deviations are small. Since the accuracy of a resonance frequency measurement at 1000 Hz is 0·1 Hz, the error on an effective length of 10 cm is 0·01 mm which is much better than the geometrical uncertainty.

4. CIRCULAR FLANGES

Figure 7(a) shows some results from the literature. The fit formula obtained experimentally by Benade and Murday [7] for a cylindrical flange of varying diameter is plotted as a dashed line. Analytical results by Ando [8] corrected by Bernard and Denardo [9] are indicated by triangular symbols. Peter *et al.* [5] did measurements for relatively thin flanges; these are also plotted in Figure 7(a). Nederveen (1998) reported preliminary results obtained by a finite difference calculation (FDM), which also are plotted in Figure 7(a). Measurements of Denardo and Bernard [27] for $a/b = 0{\cdot}33$ indicated a coefficient of about 0·82. The various results do not agree much.

4.1. ZERO AND LOW-FREQUENCY LIMIT

4.1.1. *Results with FDM*

One question about circular flanges is whether the thickness has an influence on the length correction. This was investigated by the FDM. Two cases were considered: one where the flange is a "thick" wall (as in Figure 1(b)) and one where it consists of a disk of minimal thickness (as shown in Figure 1(a)). In the latter case, its thickness was one mesh element, which, dependent on the number of points applied, is between 0·1 and 0·05 of the radius. Results for the thin disk as a flange are not very different from those of a thick wall (see Figure 7(b) and Table 1) showing that the thickness of the flange is a parameter which does not have a large influence on radiation impedance. The difference between thick and thin flanges was also studied with BEM and it was also found that the differences are small. The overall accuracy in δ is estimated to be $\pm 0{\cdot}3\%$.

4.1.2. *Results extrapolated from BEM*

As the BEM is not valid for low frequencies, results cannot be directly compared with those of the FDM. However, after the correction with the function g (equation (39)), the slope of the curve at low frequencies is nearly horizontal which allows one to extrapolate results to zero frequency. Results are plotted in Figure 7(b) and are in good agreement with FDM.

4.1.3. *Formula*

From the FDM results a fit formula was deduced for the the length correction:

$$\delta_{circ} = \delta_\infty + \frac{a}{b}(\delta_0 - \delta_\infty) + 0{\cdot}057\,\frac{a}{b}\left[1 - \left(\frac{a}{b}\right)^5\right] a. \tag{41}$$

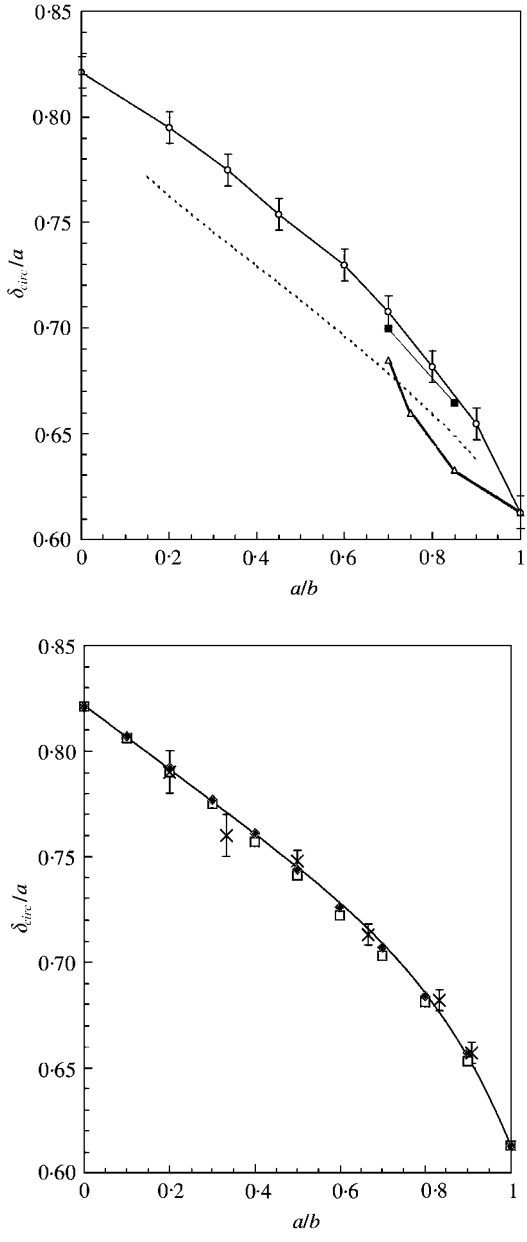

Figure 7. Real part of the end correction coefficient δ/a for a flat circular flange. (a) Literature results; ------, Benade and Murday [7]; △, Ando [8] and Bernard and Denardo [9]; ■, Peters *et al.* [5]; ○, Nederveen [12]. (b) Results with FDM for thin and thick flange and extrapolated results from BEM. □, FDM, thin circular flange; ◆, FDM, thick circular flange; ——, fit formula; ×, BEM extrapolated.

Here, $\delta_\infty = \delta(a/b = 0) = 0{\cdot}8216a$ and $\delta_0 = \delta(a/b = 1) = 0{\cdot}6133a$. The accuracy is estimated to be better than $\pm 0{\cdot}01a$. This equation can be interpreted as a linear interpolation between the two extreme values for the infinitely and unflanged pipe, with a higher order correction term of less than 5%.

TABLE 1

End corrections for various flanges obtained by the FDM; listed are δ/a = *length correction/pipe radius; for a square pipe the radius a is an "effective" value calculated from* a = *pipe width*$/\sqrt{\pi}$

	A	B	C	D	E
a/b	Thick circular flange	Thin circular disk	Sphere	Cylinder	Square flange
0	0·821	0·821	0·821	0·821	0·810
0·1	0·807	0·806	0·760	0·750	0·795
0·2	0·792	0·790	0·725	0·690	0·780
0·3	0·777	0·775	0·700	0·650	0·764
0·4	0·761	0·757	0·685	0·610	0·747
0·5	0·744	0·741	0·670	0·560	0·730
0·6	0·726	0·722	0·655	0·515	0·711
0·7	0·707	0·703	0·646	0·455	0·691
0·8	0·684	0·681	0·637		0·668
0·9	0·657	0·653	0·625		0·640
1·0	0·613	0·613	0·613		0·597

4.2. FREQUENCY DEPENDENCE

4.2.1. *Frequency dependence estimation with BEM and measurements*

Measurement have been carried out with flanges of various diameters b (b = 11, 12, 15, 20, 30 and 50 mm) fixed on the same tube of length 85 mm, wall thickness 1 mm and inner radius a = 10 mm. Each flange has the same thickness of 10 mm except for b = 11 mm which corresponds to an "unflanged tube" of thickness 1 mm. These dimensions correspond to those calculated with BEM. Results appear to be in good agreement with measurements for every diameter, for the imaginary part of the reflection coefficient as well as for the real part (see Figure 8). For reference the results for, respectively, the infinite flange and the unflanged case (equations (13) or (14) and (15)) are also plotted in Figure 8.

Oscillations visible in the curves of Figure 8 appear to be related to the radius of the flange. In reference [27] Bernard and Denardo found a value of $0{\cdot}82\,a$ for the length correction. This was for $a/b = 0{\cdot}33$ and for $ka \cong 0{\cdot}15$. This value corresponds more or less to results obtained with BEM. For small thickness, real parts of radiation impedance are very close to the unflanged case for low frequencies. For larger flanges it appears that the low-frequency limit always equals the value for the unflanged case and the high-frequency limit equals that for the infinite flange case. This can be easily explained. Upon assuming $ka \ll 1$ and $kb \ll 1$ a compact region can be defined in which a radial symmetrical flow can be established outside the pipe. By using mass and energy conservation in this region the plane wave solution in the pipe and the spherical wave solution in the far field outside the pipe can

Figure 8. Radiation impedance versus frequency for circular flanges of various radii. Upper, Length correction δ over inner radius a; lower, absolute value of the logarithm of the modulus of the reflection coefficient over $(ka)^2/2$. (a) $a/b = 10/11$; (b) $a/b = 5/6$; (c) $a/b = 2/3$; (d) $a/b = 1/2$; (e) $a/b = 1/3$; (f) $a/b = 1/5$. ·····, Theory for infinite flange [upper, equation (15)] and unflanged case [lower, equation (13)]; + + + +, calculation with BEM; ——, experimental results; -------, fit formula (equations (41), (42)); • • •, Ando [8] and Bernard and Denardo [9] results (figure 8(a) and 8(b) only).

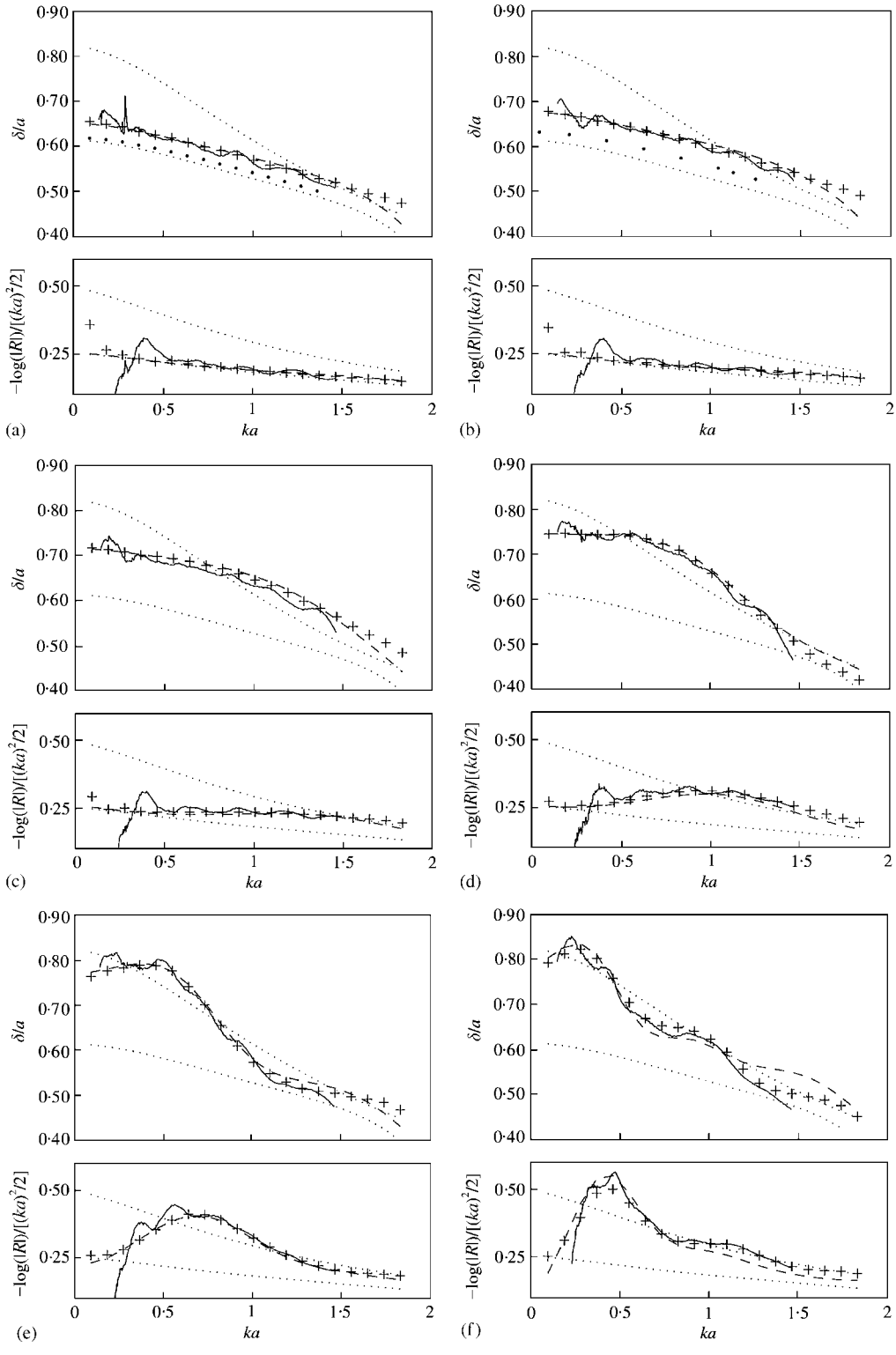
δ/a
0·90
0·80
0·70
0·60
0·50
0·40
−log(|R|)/[(ka)²/2]
0·50
0·25
0
0·5
1
1·5
2
ka
(a)
(b)
(c)
(d)
(e)
(f)

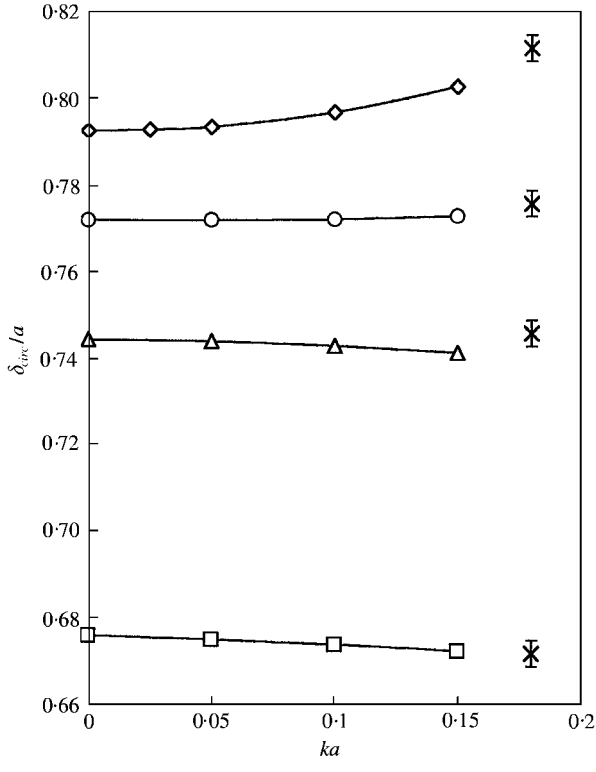

Figure 9. End correction coefficient δ/a for a flat circular flange as a function of ka. ◇, $a/b = 1/5$ (FDM); ○, $a/b = 1/3$ (FDM); △, $a/b = 1/2$ (FDM); □, $a/b = 5/6$ (FDM); ×, BEM.

be matched leading to $-\log|R| = (ka)^2/2$. Upon assuming $ka \ll 1$ and $kb \gg 1$ the real part of the pipe radiation impedance is doubled because the plane wave solution matches to a half-spherical wave outside (see for example reference [28] pp. 41–42).

4.2.2. *Low-frequency dependence with FDM and BEM*

The BEM fails below $ka = 0{\cdot}15$ and the FDM loses accuracy above this value. However, results appear to fit well in this region as can be seen from Figure 9 where real parts of the end corrections are plotted, as obtained by BEM at $ka = 0{\cdot}18$ and by FDM for $ka \leqslant 0{\cdot}15$. The results correspond within 1% of δ.

4.2.3. *Formula*

To construct a fit-formula the observation from Figure 8 that oscillations are probably caused by a reflection at the edge of the flange (see Figure 1(c)) is used. This reflection can be modelled as a reflection coefficient R_{edge} which has to be added to the reflection coefficient $R_{noref\,l}$ in the absence of reflection at the edge of the flange. The reflection coefficient R_{circ} for the circular flange is assumed to be given by

$$R_{circ} = R_{noref\,l} + R_{edge}. \tag{42a}$$

The reflection coefficient $R_{noref\,l}$, upon writing $\tilde{\delta}_{noref\,l}{}^* = \mathrm{j}\ln(-R_{noref\,l})/(2k)$, is assumed to be given by formula (41) with complex and frequency-dependent values for the length

corrections $\tilde{\delta}_\infty{}^*$ and $\tilde{\delta}_0^*$ which can be deduced, respectively, from equations (15) and (13) or equation (14) (as $\tilde{\delta}^* = \tilde{\delta} + \mathrm{j}\ln(|R|)/(2k)$).

After trial and error the following expression for the reflection coefficient R_{edge} was found:

$$R_{edge} = -0{\cdot}43\,\frac{(b-a)\,a}{b^2}\sin^2\left(\frac{kb}{1{\cdot}85 - a/b}\right)\mathrm{e}^{-\mathrm{j}kb[1\,+\,a/b(2{\cdot}3\,-\,a/b\,-\,0{\cdot}3(ka)^2)]}. \tag{42b}$$

where k is the wave number.

The accuracy for the equivalent length correction $\tilde{\delta}_{circ}$ (calculated by $\tilde{\delta}_{circ} = \mathrm{Re}[\mathrm{j}\ln(-R_{circ})/(2k)]$) is estimated to be better than $\pm 0{\cdot}02a$. The accuracy in the modulus of the reflection coefficient $|R_{circ}|$ is estimated to be better than $\pm 1\%$. This is valid for $a/b \geqslant 0{\cdot}2$, $ka < 1{\cdot}5$ and $kb < 3{\cdot}5$. This function is plotted for different values of a/b in Figure 8.

5. SQUARE AND NORMALIZED FLANGES

5.1. SQUARE FLANGE ON A SQUARE TUBE

Wooden organ pipes usually have a square section and, the thickness of the pipe wall being constant, they end with a square flange. Seen from the axis of the pipe, the ratio a/b is the same in every direction. An obvious estimate of the end correction is therefore that of a cylinder with the same cross-section and the same thickness. For a square pipe with a half-width a_{sq}, the inner radius of this substitution cylinder is $a_{eff} = 2a_{sq}/\sqrt{\pi}$ and the outer radius $b_{eff} = 2b_{sq}/\sqrt{\pi}$.

An approximation for the radiation length correction can be obtained by assuming the flow to be perfectly radial. In that case, the inertance of the end (proportional to the end correction) can be found by adding the reciprocal inertances of thin slices, of which the values are known from the circular flange. Since the value of a/b in every direction is the same, this calculation can be done analytically. Since cross-flow is neglected, the thus obtained value will be too high [22, pp. 343 and 29].

To calculate the correction without this systematic error, the FDM was used. Because of symmetry, a segment of 45° was sufficient. In this segment a three-dimensional Cartesian network was generated. Compared with the previous calculations, the number of points was much higher. To obtain accurate results, many situation with different numbers of points over the width of the channel and different amounts of stretch needed to be investigated. For a/b values of 0 and 1 the same procedure was used as described for the circular flange. Values for $a/b = 0{\cdot}1$ and $0{\cdot}9$ were rather inaccurate. Their accuracy was improved by comparison with the radial flow values and by interpolation between adjacent values. The error in the results is estimated to be $\pm 1\%$. Results are given in Table 1 and in Figure 10. The following fit equation is useful:

$$\delta_{sq} = \delta_{sq\infty} + \frac{a}{b}(\delta_{sq0} - \delta_{sq\infty}) + 0{\cdot}057\,\frac{a}{b}\left[1 - \left(\frac{a}{b}\right)^5\right]a_{eff}. \tag{43}$$

Here $\delta_{sq\infty} = 0{\cdot}811a_{eff}$ and $\delta_{sq0} = 0{\cdot}597a_{eff}$.

The difference with the values for the circular flange is less than 3%. This suggests that formulas for similarly shaped flat flanges such as ellipses or rectangles will be approximately the same.

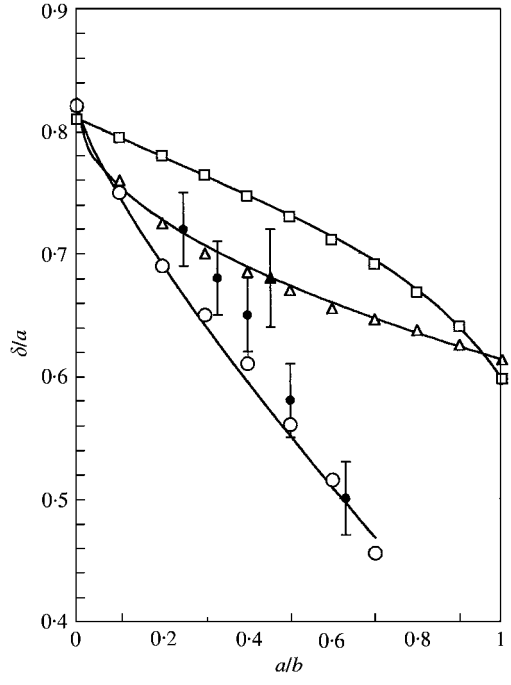

Figure 10. Length correction coefficient for a square flange, a spherical flange and a cylindrical flange as a function of the tube/flange diameter ratio; △, Sphere (FDM); ▲, sphere (experiment); □, flat square (FDM); ○, cylinder (FDM); ●, cylinder (experiments); ——, fit formulas.

5.2. NORMALIZED RECTANGULAR FLANGE ON A CIRCULAR PIPE

For loudspeaker characterization a normalized rectangular flange is used [30]. Its dimensions, given in Figure 1(d), are such that there is no simple ratio between any of the dimensions, apparently to avoid resonances due to reflections at edges.

Because this flange has no symmetry axis, and a 3-D FDM mesh would mean an even larger number of nodes than in the previous case, some alternative ways were used to find an approximate solution. An obvious simplification is replacing the rectangular flange with area S with a circular one with radius b with the same area S according to $b = (S/\pi)^{1/2}$. This gives $a/b = 0{\cdot}119$, which, upon applying equation (41), corresponds to an end correction of $\delta = 0{\cdot}804a$. Another way of obtaining an approximation is, as was done in the previous case, adding the reciprocal inertances of a large number of slices for each of which the inertance was set equal to the value for a circular flange. This was done for 72 slices over the circumference. This yielded an end correction of $\delta = 0{\cdot}803a$. For an estimate of the possible error in this calculation one can compare the results with those obtained for the cylindrical flange by the two methods (see section 6.2). For the cylinder, for the present a/b, a deviation of about 0·003 was observed. This leads to a most likely value of $\delta_{norm} = 0{\cdot}800a$. The following formula for the normalized flange is proposed:

$$\delta_{norm} = (0{\cdot}975 \pm 0{\cdot}01)\,\delta_{\infty}. \tag{44}$$

The difference with an infinite flange is small.

Results with BEM for this shape were insufficiently accurate. A measurement was carried out with the same tube as for circular flange. Results show that the infinite flange theoretical curve and measurements are very similar, showing that the normalized flange can be

considered as a good approximation of the infinite flange (see Figure 2 upper). The modulus of the reflection coefficient $|R|$ seems to be close to the one for the infinite flange (see Figure 2 lower). In fact, for the very low frequencies it may tend to the value for the unflanged case ($\ln(|R|) = (ka)^2/4$ instead of $\ln(|R|) = (ka)^2/2$) but in that case these quantities are very small and may be neglected. It can be concluded that the normalized flange is a rather good approximation of the finite flange and that equation (44) can be used with a complex and frequency-dependent value of the infinite flange length correction (equation (15) with $\tilde{\delta}^*_\infty = \tilde{\delta}_\infty + \mathrm{j}\ln(|R_\infty|)/(2k)$).

6. SPHERICAL AND CYLINDRICAL FLANGES

6.1. SPHERICAL FLANGES

Results obtained by FDM for a flange in the form of a sphere, as can be found on some wind instruments (English horn for example), are plotted in Figure 10, with triangles. Accuracy is estimated to be $\pm$ 3%. The following fit-formula is drawn through the points:

$$\delta_{sph} = \delta_\infty + \frac{a}{b}(\delta_0 - \delta_\infty) - 0{\cdot}11\left(\frac{a}{b}\right)^{1/3}\left(1 - \frac{a}{b}\right)a. \tag{45}$$

One case was investigated experimentally: for $a/b = 0{\cdot}45$ this gives the value $\delta_{sph} = (0{\cdot}68 \pm 0{\cdot}04)a$ which agreed with FDM results. Frequency dependence is intermediate between frequency dependence for the finite flange and the unflanged case. In fact, a spherical flange is not expected to exhibit an oscillatory behaviour in the reflection coefficient as encountered in the case of the thin flange since it has no sharp edge. This suggests that equation (45) may also be used for higher frequencies up to $ka < 1{\cdot}5$ (with $\tilde{\delta}_\infty$ and $\tilde{\delta}_0$ instead of δ_∞ and δ_0 respectively).

6.2. CYLINDRICAL FLANGES

For FDM calculations on cylindrical flanges, the domain was cut in the angular slices and the two-dimensional situation was extended with terms interconnecting the slices, creating conditions for the three-dimensional situation. Because of symmetry, a domain of 90° suffices. The flanges in the slices were parts of spheroids, for which the conditions were modifications of those of the spherical flange of the previous case. Results are shown in Figure 10, with circles, and the line drawn through the points is the fit formula valid for $a/b < 0{\cdot}7$:

$$\delta_{cyl} = \delta_\infty - 0{\cdot}47\,(a/b)^{0{\cdot}8}. \tag{46}$$

Estimated accuracy is estimated to be $\pm$ 5%. To verify the 3-D procedure, the flow was approximated by taking the mean value of results from 2-D flow in the slices. As mentioned above, the values thus obtained are expected to be somewhat higher. This amounts to about 1% for low values of a/b and about 7% for the highest value of 0·7.

Experiments were carried out for different values of the cylinder radius b. Results extrapolated to zero frequency are shown in Figure 10 for different values of a/b ($a/b = 0{\cdot}63$; 0·5; 0·4; 0·33; 0·25). Agreement with numerical calculation is not very good, the difference being 10% for $a/b = 0{\cdot}25$. This requires further investigation.

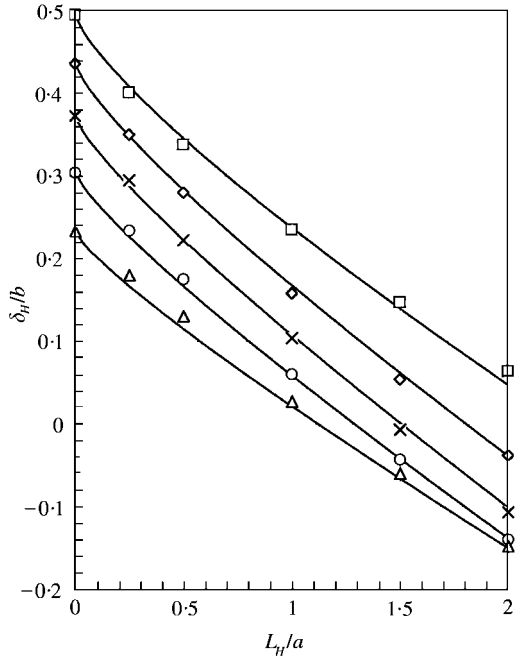

Figure 11. End correction coefficient δ_H/b for a tube with a short catenoidal horn as a function of the reduced horn length L_H/a (FDM calculations). □, $a/b = 0{\cdot}7$; ◇, $a/b = 0{\cdot}6$; ×, $a/b = 0{\cdot}5$; ○, $a/b = 0{\cdot}4$; △, $a/b = 0{\cdot}3$; ——, fir formulas.

7. QUICKLY FLARING SHORT HORNS

Some instruments (saxophones, for example) have a quickly flaring short horn (see Figure 1(g)). Most horns are nearly catenoidal. For this horn, the radius r is given by $r = a\cosh(x/h)$, where a is the throat radius, x the distance to the throat of the horn and h a constant. The finite difference method was employed to find an end correction for such horns. Although saxophones are conical, the horn flares quickly enough for one to assume that the value obtained for a horn onto a cylinder will be approximately the same as that on a cone. Results are plotted in Figure 11 versus total horn length divided by the throat radius a. Note that the end correction is applied to the horn end which means that at wider horns the correction can become negative. The length correction is referred to the outer radius of the horn b. Drawn lines are according to the following fit formula, valid for $L_H/a \leqslant 2$ and $0{\cdot}3 \leqslant a/b \leqslant 0{\cdot}7$:

$$\delta_H = \left(\frac{\tanh(\operatorname{arc\,cosh}(b/a))}{\operatorname{arc\,cosh}(b/a)} - 1\right) L_H + \frac{\delta_{circ}\, a}{1 + 0{\cdot}28\,(L_H/a)^{0{\cdot}7}\,(a/b)^{-1/4}}. \tag{47}$$

The first term is the value for a long catenoidal horn with a zero-impedance termination (see for example reference [12]). The second term is a correction due to the flaring open end. A measurement was carried out for a short catenoidal horn where $L_H/a = 1$ and $a/b = 0{\cdot}5$. The frequency dependence appeared to be much more intricate than for the infinite flange or the unflanged pipe. Therefore, the zero frequency value obtained by extrapolation to zero is rather uncertain. The length correction obtained for this horn was $\delta_H = (0{\cdot}2 \pm 0{\cdot}1)\,a$ which is in good agreement with the FDM result ($\delta_H = 0{\cdot}1b = 0{\cdot}2a$).

TABLE 2

Survey of FDM *calculations for disk above open end; numbers are numver of elements used*

Figure	Inner radius a	Wall thickness w	Disk radius d	Disk thickness e	Diskhole radius q
9	40	10	66	16	0
9	40	8	59	16	0
9	40	4	55	16	0
9	40	2	53	16	0
9	40	1	52	16	0
10	40	4	55	16	0
10	40	4	55	4	10
10	40	4	55	16	10
10	40	4	55	4	20
10	40	4	55	16	20

8. KEY HANGING ABOVE A HOLE, WITH AND WITHOUT A PERFORATION

A disk or key positioned at a certain distance above a hole increases the end correction notably. The most important parameter is the distance to the rim of the hole. Others are the wall thickness of the chimney the key is hanging above, the key dimensions and the optional hole in this key. Figure 12 shows the nomenclature for the various parameters. Table 2 lists the situations investigated. In Figure 13, the extra effect due to the presence of a disk without a hole is plotted versus the lift height of the disk. The results and those in Figure 14 are plotted on a double logarithmic scale, which appear to present results better than with one or both axes linear. The common range for the value h/a on wind instruments is between 0·1 and 1. Roughly approximated, the end correction is inversely proportional to h/a, with deviations at the extremes of the range. The magnitude of the effects can be seen in the diagram. When the key is close to the hole it adds an important extra length to the hole, between one and two times its radius. When the key is further away, the correction can be about $0{\cdot}05a$ which is small but not negligible. Various wall thicknesses were studied. FDM results are plotted with circles. Lines are corresponding fit formulas according to

$$\delta_{disk} - \delta_{circ} = \frac{a}{3{\cdot}5(h/a)^{0{\cdot}8}(h/a + 3w/a)^{-0{\cdot}4} + 30(h/d)^{2{\cdot}6}}, \tag{48}$$

where w is the wall thickness and d the radius of the disk. δ_{circ} is the value of the length correction without disk. It is given by equation (41) with $b = a + w$. The thickness of the disk e was varied, but it was found to have only a minor influence, so it is not included in the formula. Experiments, based on resonance frequency measurements, have been carried out with $a = 10\,\text{mm}$, $w = 1\,\text{mm}$ and $d = 13{\cdot}75\,\text{mm}$. Results are shown with plus-symbols in Figure 13 and appear to be in good agreement with the proposed fit formula. This formula is applicable in the range for which it is plotted in Figure 13.

For a key with a perforation, the dimensions investigated are listed in Table 1. Some results obtained with the FDM are shown in Figure 14. To construct a fit formula, it was speculated that the disk hole impedance plays an important role. The end correction was chosen as a parameter to be applied when the key is closed (that means that $h = 0$). This end correction can be calculated from well-known formulae. The length of the hole consists of its physical length e and two end corrections. The one on the outside δ_{out} is given by equation (41) with q, disk hole radius, instead of a and d, disk radius, instead of b giving $\delta_{out} = \delta_\infty + q/d(\delta_0 - \delta_\infty) + 0{\cdot}057q/d[1 - (q/d)^5]q$ with $\delta_\infty = 0{\cdot}822q$ and $\delta_0 = 0{\cdot}613q$. The

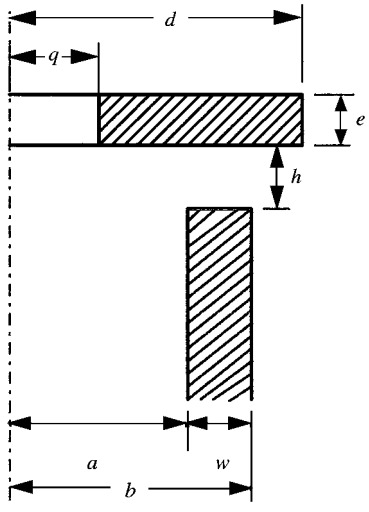

Figure 12. Dimension definition for a disk (key) above an open end.

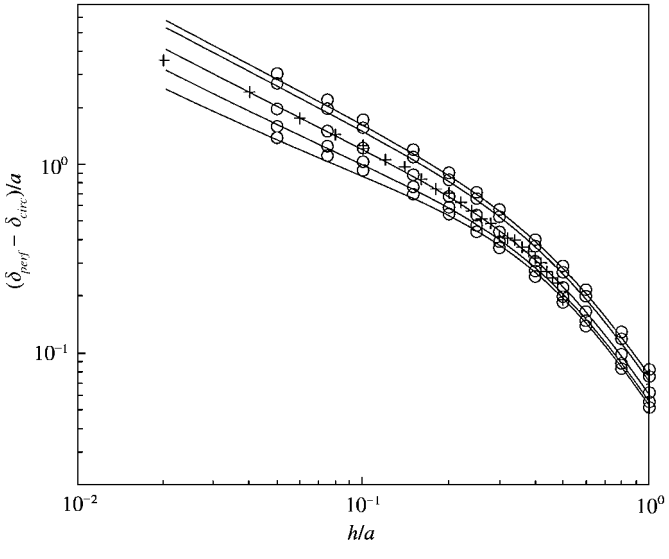

Figure 13. Dependence of the change in the end correction coefficient $(\delta_{disk} - \delta_{circ})/a$ versus the relative distance h/a for various wall thickness w (from top to bottom $w/a = 0{\cdot}25, 0{\cdot}2, 0{\cdot}1, 0{\cdot}05$ and $0{\cdot}025$). ○, FDM calculations; +, experiment for $w/a = 0{\cdot}1$; ——, fit formula.

inside correction δ_{in} is taken from a study by Kergomard and Garcia [31] for which a useful fit formula was derived by Nederveen [12] for the zero-frequency case:

$$\delta_{in} = \delta_{\infty} - 1{\cdot}1q^2/a + 0{\cdot}28q(q/a)^{3{\cdot}5}. \tag{49}$$

The effective length of the hole in the disk is $e + \delta_{in} + \delta_{out}$. This can be transformed into a length correction δ_e to be applied to the main hole:

$$\delta_e = (a/q)^2 (e + \delta_{in} + \delta_{out}]. \tag{50}$$

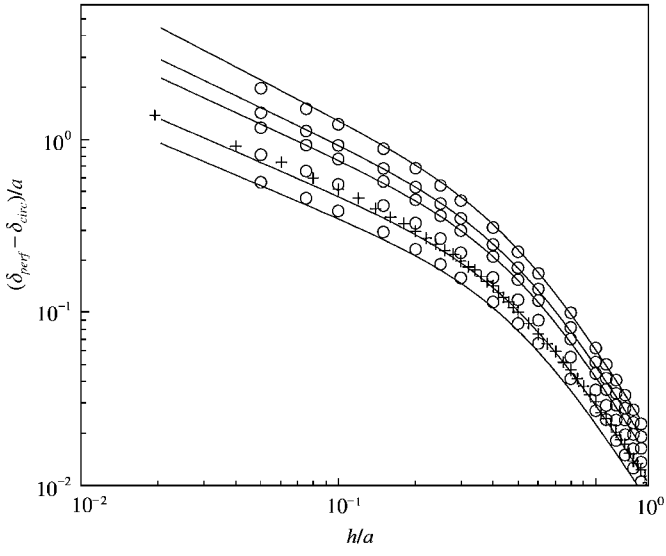

Figure 14. Dependence of the change in the end correction coefficient $(\delta_{perf} - \delta_{circ})/a$ versus the relative distance h/a for disks of various thickness e with perforations of various diameters q (from top to bottom $e/a = 0{\cdot}4$ and $q/a = 0$; $e/a = 0{\cdot}4$ and $q/a = 0{\cdot}25$; $e/a = 0{\cdot}1$ and $q/a = 0{\cdot}25$; $e/a = 0{\cdot}4$ and $q/a = 0{\cdot}5$; $e/a = 0{\cdot}1$ and $q/a = 0{\cdot}5$; see Table 1 for details). ○, FDM calculations; +, experiment for $w/a = 0{\cdot}1$; ——, fit formula.

Upon neglecting the higher order terms in equation (50) the following result for δ_e/a is obtained:

$$\delta_e/a = [1{\cdot}64a/q - 0{\cdot}15a/d - 1{\cdot}1 + ea/q^2]. \tag{51}$$

This is used in a fit formula for a perforated disk, obtained by trial and error, as follows:

$$\delta_{perf} - \delta_{circ} = \frac{\delta_{disk} - \delta_{circ}}{1 + 5(\delta_e/a)^{-1{\cdot}35}\,(h/a)^{-0{\cdot}2}}. \tag{52}$$

These function are plotted in Figure 14 for some values of e/a and q/a as indicated. They appear to describe the FDM results reasonably well, at least sufficiently accurately for practical purposes.

Experiments have been carried out with $a = 10\,\text{mm}$, $w = 1\,\text{mm}$, $q = 5\,\text{mm}$, $e = 2\,\text{mm}$ and $d = 13{\cdot}75$ mm. Results are plotted in Figure 14 with plus-symbols and appear to be in good agreement with the proposed fit formula within the range shown in the diagram. Note that some experimental results can be found in references [10, 11] which were verified to fit with the present results (see also reference [12]).

Application of the formulas in practical situations has to be done with care, since there usually are deviations from the ideal situations for which the formulas are derived. For example, in a wind instrument with side holes, the pad attached to the key is not perfectly flat, and the key pivots around an axis, due to which it does not move along the hole axis.

9. CONCLUSION

The magnitude of the radiation impedance is important when modelling open tubes. The present paper studies different types of termination (flanges) and gives, for each type, fit formulas (equations (41)–(52)). Some results are worth mentioning. For thin circular tubes

(wall thickness less than a quarter of the radius) the length correction is larger than reported in the literature [8, 9]. For circular flanges results show that the reflection at the edges of the flange have a notable influence. A fit formula based on an estimate of this reflection appears to describe the results well. The so-called normalized flange used for loudspeaker characterization was measured and is shown to have a radiation impedance only 3% less than the theoretical impedance for the infinite flange. It is shown that the zero frequency formula for the circular flange can be applied to the case of a square tube with a square flange by using the respective values for the unflanged and infinitely flanged cases.

The methods used can in principle be applied to any other geometry although the writing of a program for intricate 3-D geometries can be difficult and the results can be inaccurate. It is shown in this paper (see also reference [30]) that the method which approximates the flow field by pure radial flow can give sufficiently good results, apart from a small systematic deviation. Many numerical results were verified with experiments. Agreement was satisfactory for the imaginary part of the impedance (length correction) as well as for the real part (losses).

ACKNOWLEDGMENTS

Thanks to M. Bernard who did the "Ando's" calculation (Figure 10(a) and 10(b) and Simon Félix and Tony Blanchard for contributing to measurements.

REFERENCES

1. L. V. King 1936 *Philosophical Magazine* **21**, 128–144. On the electrical and acoustic conductivities of cylindrical tubes bounded by infinite flanges.
2. H. Levine and J. Schwinger 1948 *Physical Review* **73**, 383–406. On the radiation of sound from an unflanged circular pipe.
3. Y. Nomura, I. Yamamura and S. Inawashiro 1960 *Journal of the Physical Society of Japan* **15**, 510–517. On the acoustic radiation from a flanged circular pipe.
4. A. Hirschberg, J. Gilbert, R. Msallam and A. P. J. Wijnands 1996 *Journal of the Acoustical Society of America* **99**, 1754–1758. Shock waves in trombones.
5. M. C. A. M. Peters, A. Hirschberg, A. J. Reijnen and A. P. J. Wijnands 1993 *Journal of Fluid Mechanics* **256**, 499–534. Damping and reflection coefficient measurements for an open pipe at low Mach and low Helmholtz numbers.
6. U. Ingard and H. Ising 1967 *Journal of the Acoustical Society of America* **42**, 6–17. Acoustic nonlinearity of an orifice.
7. A. H. Benade and J. S. Murday 1967 *Journal of the Acoustical Society of America* **41**, 1609. Measured end corrections for woodwind tone holes.
8. Y. Ando 1969 *Acoustica* **22**, 219–225. On the sound radiation from semi-infinite circular pipe of certain wall thickness.
9. M. Bernard and B. Denardo 1996 *Acoustica* **82**, 670–671. Re-computation of Ando's approximation of the end correction for a radiating semi-infinite circular pipe.
10. H. Bouasse 1929 *Tuyaux et résonateurs*. Paris: Delagrave. Reprint by Blanchard, Paris, 1986.
11. J. W. Coltman 1979 *Journal of the Acoustical Society of America* **65**, 499–506. Acoustical analysis of the Boehm flute.
12. C. J. Nederveen 1969 *Acoustical Aspects of Woodwind Instruments*. De Kalb: Northern Illinois University Press, DeKalb, III., revised edition 1998.
13. C. Zwikker and C. Kosten 1949 *Sound Absorbing Materials*. Amsterdam: Elsevier.
14. M. Bruneau 1998 *Manuel d'acoustique foundamentale*. Paris: Henmes.
15. R. Caussé, J. Kergomard and X. Lurton 1984 *Journal of the Acoustical Society of America* **75**, 241–254. Input impedance of brass instruments—comparison between experiment and numerical models.

16. J.-P. DALMONT 2000 *Journal of Sound and Vibration*. Acoustic impedance measurement. Part II: a new calibration method. [Accepted for publication.]
17. R. D. AYERS 1995 *Journal of the Acoustical Society of America* **98**, 81–87. Two effective lengths for musical wind instruments.
18. A. N. NORRIS and I. C. SHENG 1989 *Journal of Sound and Vibration* **135**, 85–93. Acoustic radiation from a circular pipe with an infinite flange.
19. S. V. PATANKAR 1980 *Numerical Heat Transfer and Fluid Flow*. London: Taylor & Francis.
20. D. ZWILLINGER 1989 *Handbook of Differential Equations*. New York: Academic Press: second edition.
21. J. K. M. JANSEN 1997 Private communication.
22. A. D. PIERCE 1989 *Acoustics. An Introduction to its Physical Principles and Applications*. New York: Acoustical Society of America.
23. M. REZAYAT, D. J. SHIPPY and F. J. RIZZO 1986 *Computational Methods in Applied Mechanics and Engineering* **55**, 349–367. On time-harmonic elastic wave analysis by the boundary element method for moderate to high frequencies.
24. M. A. HAMDI and J. M. VILLE 1986 *Journal of Sound and Vibration* **107**, 231–242. Sound radiation from ducts: theory and experiment.
25. A. BOSSAVIT 1986 *Computational Methods in Applied Mechanics and Engineering* **56**, 167–215. Symmetry, groups and boundary value problems: a progressive introduction to noncommutative harmonic analysis of partial differential equations in domains with geometrical symmetry.
26. J.-P. DALMONT and A. M. BRUNEAU 1992 *Journal of the Acoustical Society of America* **91**, 3026–3033. Acoustic impedance measurements: plane-wave mode and first helical mode contributions.
27. B. DENARDO and M. BERNARD 1996 *American Journal of Physics* **64**, 745–751. Design and measurement of variably nonuniform acoustic resonators.
28. A. HIRSCHBERG and S. W. RIENSTRA 1994 *Elements of Aero-acoustics in Applied Aero-acoustics*. Lecture series 1994-04 of the Von Karman Institute for Fluid Dynamics, Brussels, Belgium.
29. C. J. NEDERVEEN, J. K. M. JANSEN and R. R. VAN HASSEL 1998 *ACUSTICA* united with *Acta Acustica* **84**, 957–966. Corrections for woodwind tone-hole calculations.
30. IEC Standard 1980, publication 268-5.
31. J. KERGOMARD and A. GARCIA 1987 *Journal of Sound and Vibration* **114**, 465–479. Simple discontinuities in acoustics waveguides at low frequencies: critical analysis and formulae.

APPENDIX A: NOMENCLATURE

a	tube radius, m
b	flange radius, m
c	sound speed, m/s
d	disk radius, m
e	thickness of disk, m
f	frequency Hz
g	correction term for compensating low-frequency errors in BEM
G	Green function
h	grid size for finite difference calculations (section 3.1)
h	lift height of disk above hole, m
j	$\sqrt{(-1)}$
k	wave number $= \omega/c$, m
L	length, position, m
p	acoustic pressure, N/m^2 or Pa
q	radius of hole in disk, m
r	radius, m
R	reflection coefficient
R	distance to boundary (section 3.1)
S	cross-sectional area, m^2
t	temperature, °C
U	acoustic volume velocity = particle velocity times cross-section, m^3/s
V_0	normal velocity
w	wall thickness $= b - a$, m

x	position co-ordinate in tube, m
Y	acoustic admittance $= U/p$, $m^4 s/kg$
z	length co-ordinate in cylinder, m
Z	acoustic impedance $= p/U$, $kg/m^4 s$
Z_c	characteristic acoustic impedance $\cong \rho c/S$, $kg/m^4 s$
α	wall damping influence factor
δ	end correction of a tube (low-frequency limit), m
$\tilde{\delta}$	frequency-dependent end correction of a tube, m
φ	angle
ρ	density of air, kg/m^3
ω	angular frequency $= 2\pi f$ s
Ω	domain for the BEM (section 3.2)
Γ	boundary of the domain Ω for the BEM (section 3.3)

Subscripts

r	radiation
0	at abscissa 0
L	at abscissa $-L$
∞	infinitely flanged
o	unflanged
circ	circular
cyl	cylindrical flange
disk	with a disk above open end
eff	effective
H	horn
norefl	with no reflection on the edge of the flange
norm	normalized
perf	with a perforated disk above open end
sph	spherical
sq	square flange on a square tube